

Supporting Information

No growth stimulation of Canada's boreal forest under half-century of combined warming and CO₂ fertilization

Martin P. Girardin^{A*}, Olivier Bouriaud^{B,C}, Edward H. Hogg^B, Werner A. Kurz^D, Niklaus E. Zimmermann^{E,F}, Juha Metsaranta^B, Rogier de Jong^G, David C. Frank^{H,E}, Jan Esper^I, Ulf Büntgen^{E,J}, Xiao Jing Guo^A, Jagtar Bhatti^B

^ANatural Resources Canada, Canadian Forest Service, Québec

^BNatural Resources Canada, Canadian Forest Service, Edmonton

^CCurrent address: National Forest Inventory, National Institute for Research-Development in Forestry, Romania

^DNatural Resources Canada, Canadian Forest Service, Victoria

^ELandscape Dynamics, Swiss Federal Research Institute WSL, CH-8903 Birmensdorf, Switzerland

^FDept. of Environmental Systems Sciences, Swiss Federal Institute of Technology ETH, CH-8092 Zürich, Switzerland

^GRemote Sensing Laboratories, University of Zurich, Winterthurerstrasse 190, CH-8057 Zürich, Switzerland

^HLaboratory of Tree-Ring Research, University of Arizona, USA

^IDepartment of Geography, Johannes Gutenberg University, 55099 Mainz, Germany

^JOeschger Centre for Climate Change Research, Bern, Switzerland

* Corresponding author

martin.girardin@canada.ca

Introduction

The purpose of this supplementary material is to provide information that is of less central importance to the paper and that cannot be included in the main body of the text because of space limitations. The Supplementary Information contains 13 figures and 5 tables.

Table of Contents

PART A: Distribution of sampled plots and mean inter-series correlations 5

Table S1. Frequency distribution of sampled trees and plots by species in the National Forest Inventory tree-ring database. 5

Figure S1. Distribution of sampled plots in Canada’s National Forest Inventory (NFI) program. 6

Figure S2. Frequency distribution of sampled rings through time by tree genus in the National Forest Inventory tree-ring database. 7

PART B: Processing of ring width measurements 8

 B.1 Plot-level Generalized Additive Mixed Models (GAMM_{NFI}) 8

Figure S3. (A) Fitted versus observed log-scaled tree basal area increments (LBAI). The fitted values are those obtained from the plot-level fitting of the Generalized Additive Mixed Models (GAMM). (B) Residual versus fitted LBAI. (C) Same as (A) after application of the back-transformation. 8

Figure S4. Plot-level averaged basal area increments (BAI) versus ring age for a subset of data, by species. Also plotted are the plot-level averaged Generalized Additive Mixed Model (GAMM) fits used in the detrending procedure of the BAI measurement series. The residuals of these curves were used to interpret growth trends and analyze climate responses. 9

 B.2 Generalized negative exponential (GNE) procedure 16

Figure S5. (A) Fitted versus observed log-scaled tree basal area increments (LBAI). 17

 B.3 Generalized Additive Mixed Models and Regional Curve Standardization applied at the scale of ecozones 18

Table S2. Diagnostics of the ecozone-level Generalized Additive Mixed Models (GAMM). 19

PART C: Linear trends in forest growth from 1950 to 2002 20

Table S3. Linear trends in forest growth from 1950 to 2002. Analyses were performed on data originating from four methods of elimination of growth trends: species-by-plot and species-by-ecozone Generalized Additive Mixed Models (GAMM_{NFI} and GAMM_{eco}), generalized negative exponential (GNE) procedure, and Regional Curve Standardization (RCS). 21

Figure S6. Species-by-ecozone forest growth variability assessed from tree-ring measurement series for *Picea glauca* and *Abies balsamea* in the eastern Boreal Shield. 23

PART D: Relationship between normalized difference vegetation index and forest growth 24

Figure S7. Growth versus NDVI time-series. 25

PART E: Relationship between atmospheric drought and forest growth 26

Figure S8. Spatial distribution of trends in A) spring (March-May, trends expressed in °C yr⁻¹), B) summer (June-August) and C) fall (September-November) mean temperature, and D) total winter snowfall (December-May, mm of water yr⁻¹) across sampled NFI locations from 1950 to 2002 27

Figure S9. Spatial distribution of trends in A) relative humidity (% yr⁻¹) and B) vapor pressure deficit (VPD, kPa yr⁻¹) for the summer months of June to August across Canada from 1950 to 2002 28

PART F: Linear mixed models for climate sensitivity 29

Table S4. Means of the Pearson correlations between explanatory variables. 30

Table S5. Proportion (%) of the subset-averaged coefficients that exceeded the 95% adjusted confidence intervals..... 31

Figure S10. Spatial distribution of correlations between interpolated forest growth (GAMM_{NFI}) and changes predicted by the linear mixed models. GAMM_{NFI} and predictions were interpolated to 1° x 1° grids to obtain continuous yearly raster maps of predicted growth covering 1950 to 2002. 32

Figure S11. Species-by-ecozone linear mixed model 95% adjusted confidence intervals for the influence of atmospheric CO₂ concentrations on basal area increment..... 33

PART G: Additional material 34

Figure S12. Spatial distribution of forest growth trends across Canada. Tree data were processed through pre-selected plot-level Generalized Additive Mixed Models 35

Figure S13. Spatial distribution of forest growth trends across Canada. Tree data were processed through ecozone-level Generalized Additive Mixed Models 35

References 36

PART A: Distribution of sampled plots and mean inter-series correlations

The tree-ring width series collection is based on increment cores from 19 tree species sampled in Canada's National Forest Inventory (NFI) plot survey (1) (Table S1; Figs. S1 and S2). Samples were processed using standard methods, and annual ring widths were measured using either a VELMEX measuring system interfaced with a computer or the Coorecorder/CDendro software suite with a flatbed scanner (2). Measurements were taken at the Laurentian Forestry Centre, Québec, and at the Northern Forestry Centre, Edmonton, of the Canadian Forest Service. For each measurement series, cross-dating (3) and measurements were statistically verified using the COFECHA program (4). This verification procedure was applied at the levels of individual plots, of multiple-plot aggregates (e.g., 1.0° x 1.0° grids), and of ecoregions (5). Quality of measurements was also verified at the plot level using a modified form of the "Proportion of last two years growth" (P2Yrs) method (2), and at the regional scale through comparison with existing networks of tree-ring chronologies (6); (7), (8).

Table S1. Frequency distribution of sampled trees and plots by species in the National Forest Inventory tree-ring database.

Species	<i>n</i> Plots	<i>n</i> Trees
<i>Abies balsamea</i>	70	176
<i>Abies lasiocarpa</i>	31	95
<i>Acer rubrum</i>	18	53
<i>Acer saccharum</i>	5	20
<i>Betula alleghaniensis</i>	7	19
<i>Betula papyrifera</i>	12	39
<i>Larix laricina</i>	42	97
<i>Picea engelmannii</i>	9	21
<i>Picea glauca</i>	106	289
<i>Picea mariana</i>	326	1234
<i>Pinus banksiana</i>	67	199
<i>Pinus contorta</i>	44	160
<i>Pinus strobus</i>	8	21
<i>Populus balsamifera</i>	9	19
<i>Populus tremuloides</i>	69	184
<i>Pseudotsuga menziesii</i>	4	19
<i>Thuja occidentalis</i>	25	111
<i>Thuja plicata</i>	11	27
<i>Tsuga heterophylla</i>	10	24

Growth in Canada's boreal forest

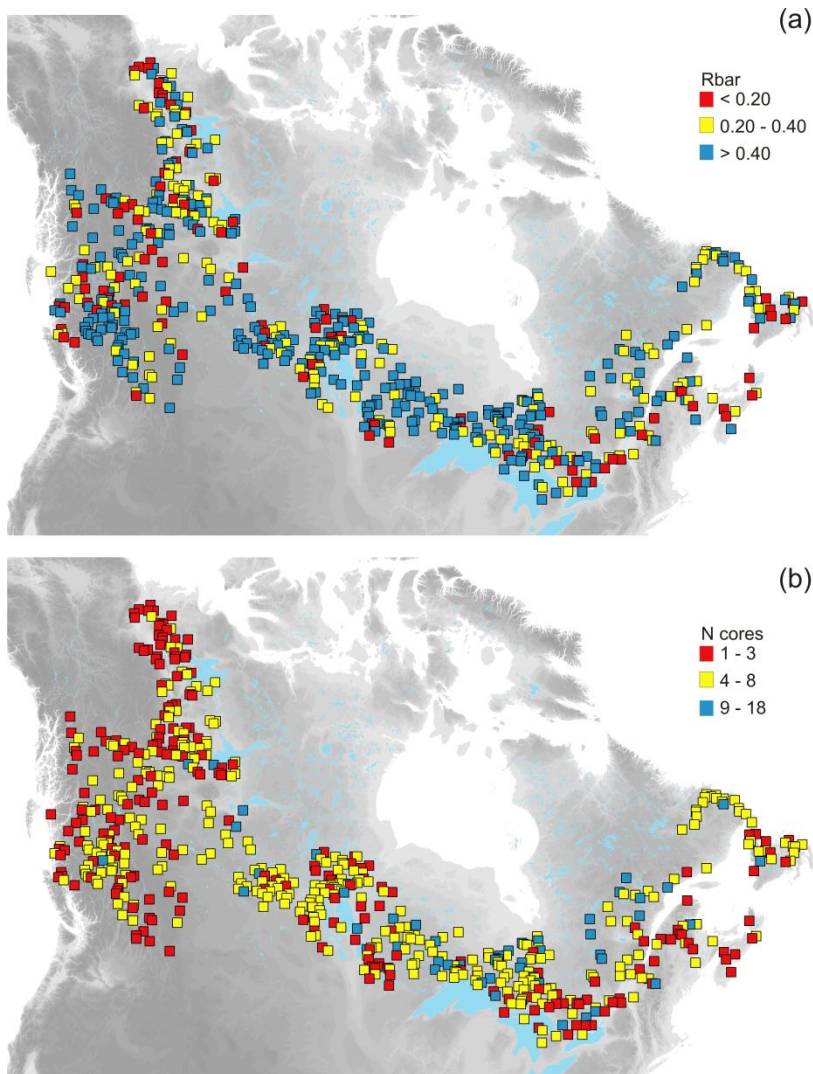


Figure S1. Distribution of sampled plots in Canada's National Forest Inventory (NFI) program. a) Mean inter-series correlation (R_{bar}) of single-plot chronologies. Inter-series correlations were computed on Generalized Additive Mixed Models (GAMM) normalized residuals at the species-level within a plot, and then averaged at the plot level. A high R_{bar} denotes high synchronicity in the growth of trees within a NFI plot. If a given plot contains only one tree, then the R_{bar} was computed using trees from the same ecoregion (61 cases). The median R_{bar} is 0.41. b) Number of cores (N_{cores}) available in each NFI plot.

Growth in Canada's boreal forest

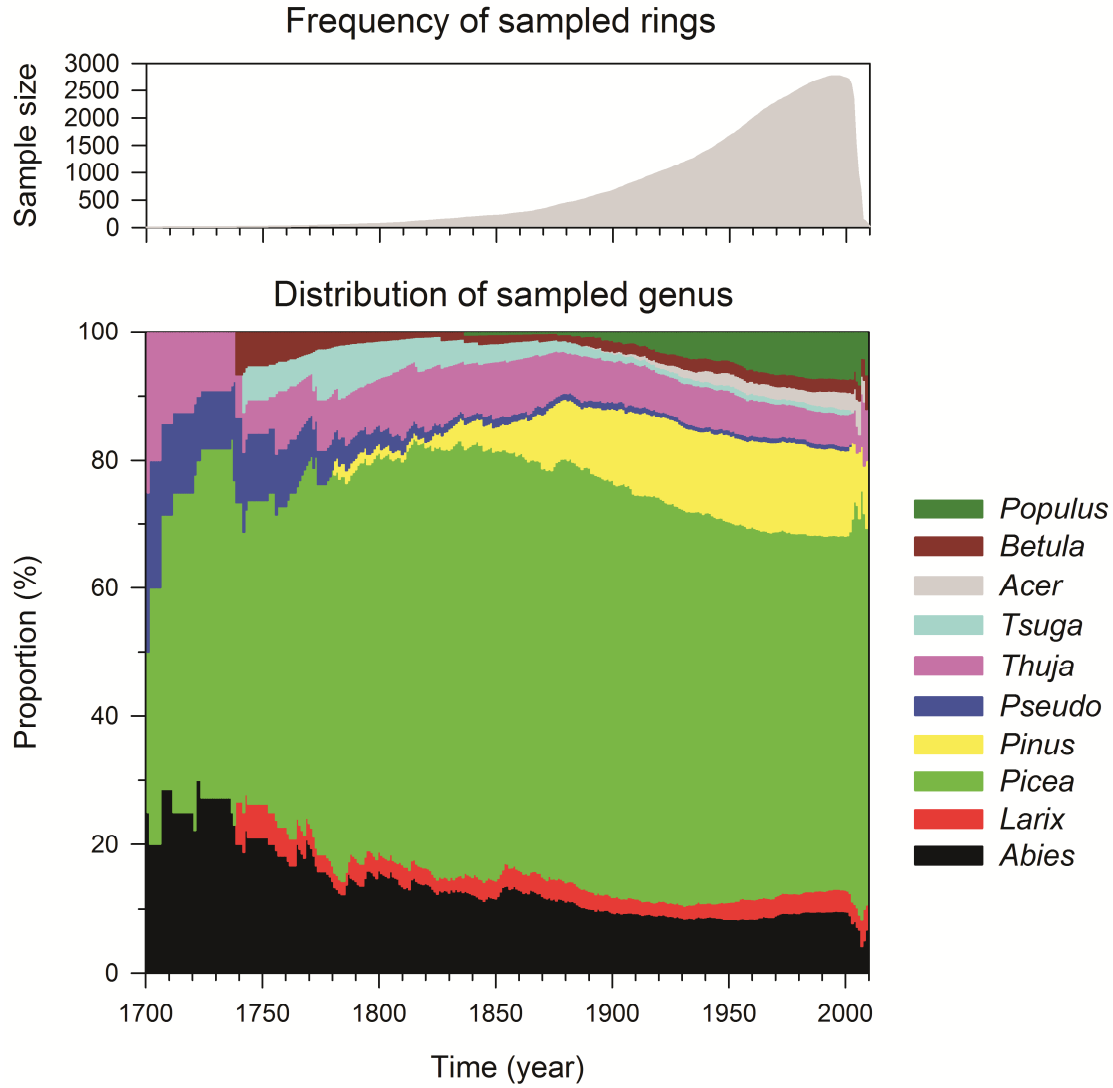


Figure S2. Frequency distribution of sampled rings through time by tree genus in the National Forest Inventory tree-ring database.

PART B: Processing of ring width measurements

B.1 Plot-level Generalized Additive Mixed Models (GAMM_{NFI})

We used the Generalized Additive Mixed Models (GAMM; (9)) approach (10) to remove intrinsic effects for each species-by-plot combination (873 analyses in total). This approach makes it possible to model BAI as a function of cambial age and tree basal area. Below are shown biplots (Fig. S3) and time-series curves of the fitted versus observed tree basal area increments (Fig. S4) generated from the plot-level GAMM_{NFI} approach.

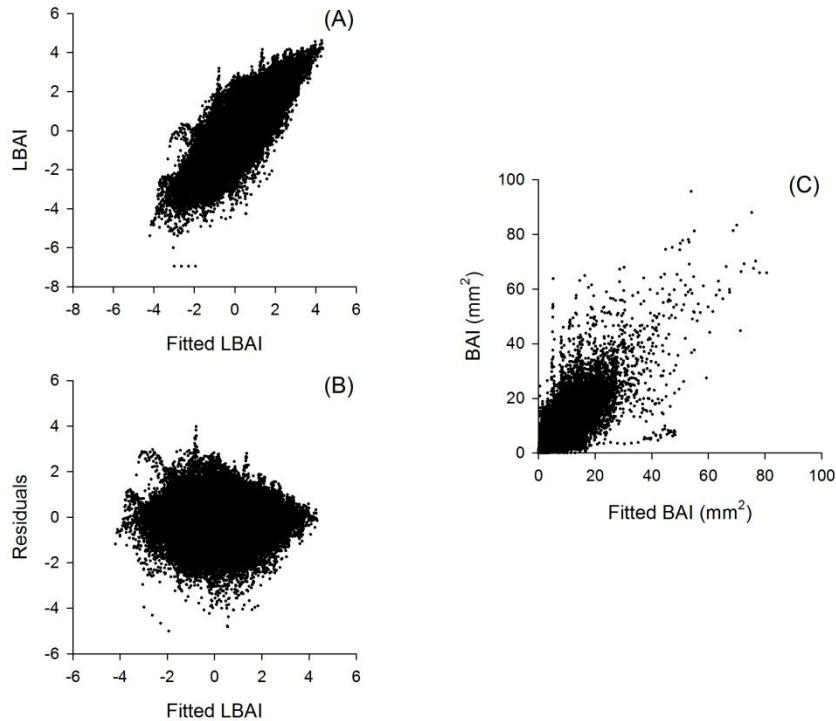


Figure S3. (A) Fitted versus observed log-scaled tree basal area increments (LBAI). The fitted values are those obtained from the plot-level fitting of the Generalized Additive Mixed Models (GAMM). (B) Residual versus fitted LBAI. (C) Same as (A) after application of the back-transformation into BAI using the approach described by (11) (see Methods).

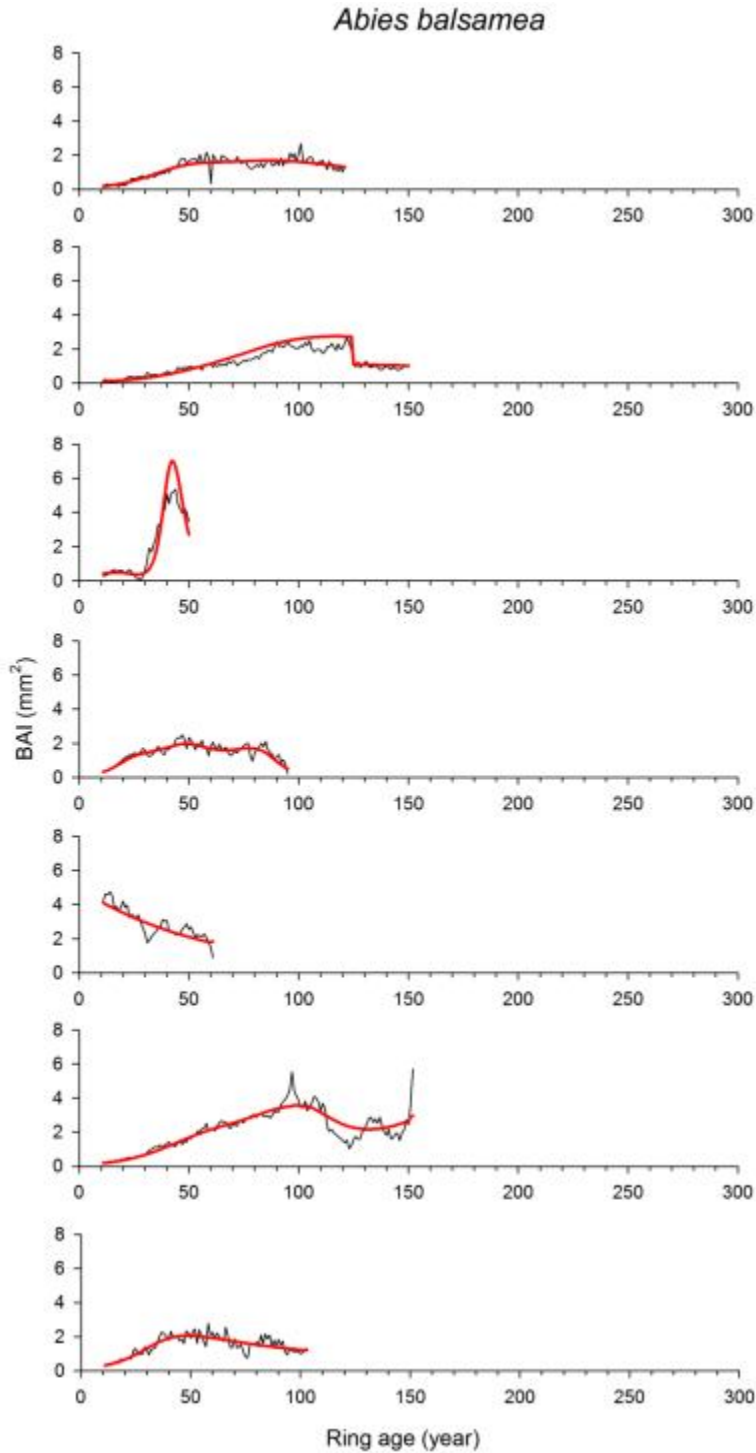


Figure S4. Plot-level averaged basal area increments (BAI) versus ring age for a subset of data, by species. Also plotted are the plot-level averaged Generalized Additive Mixed Model (GAMM) fits used in the detrending procedure of the BAI measurement series. The residuals of these curves were used to interpret growth trends and analyze climate responses. (*Continues on the next pages*)

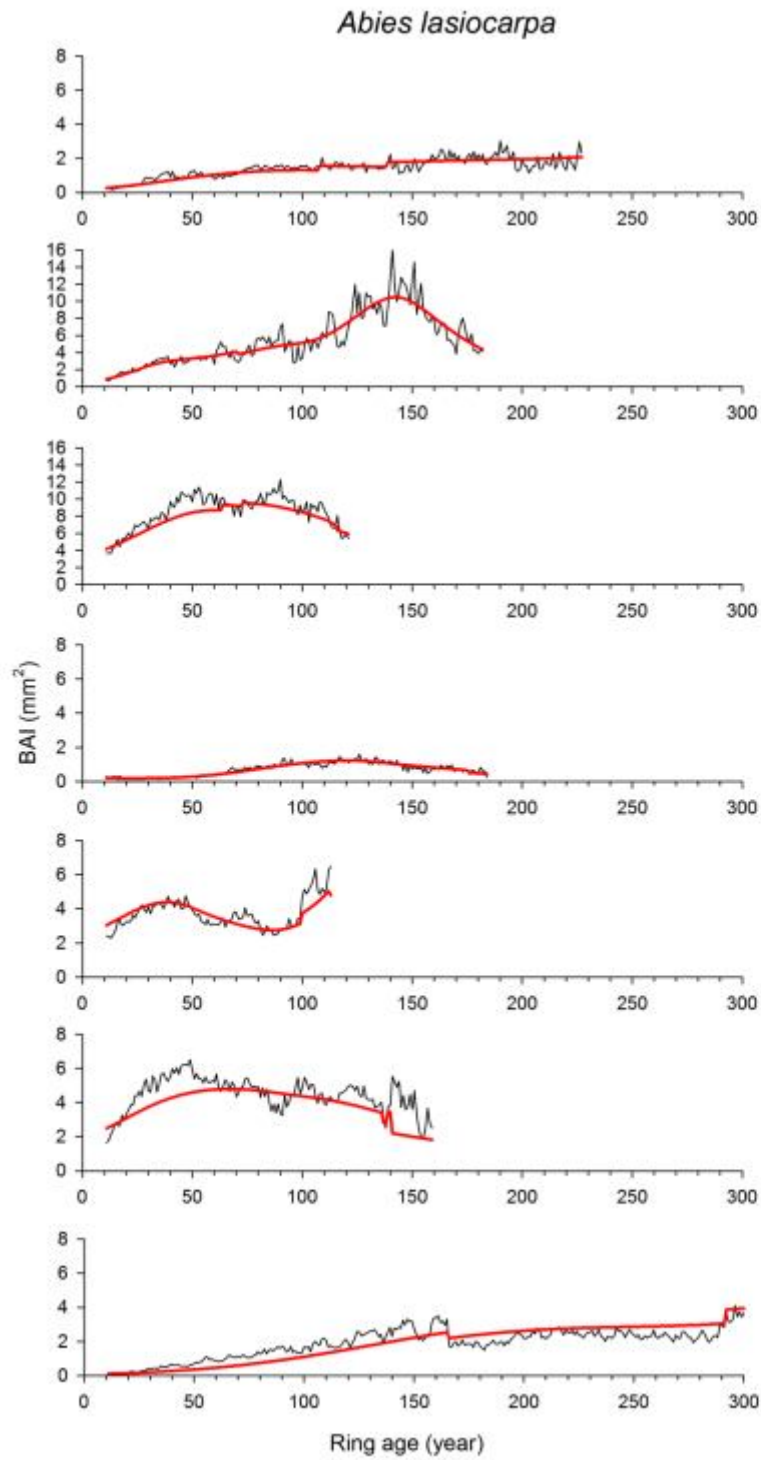


Figure S4. *Continues*

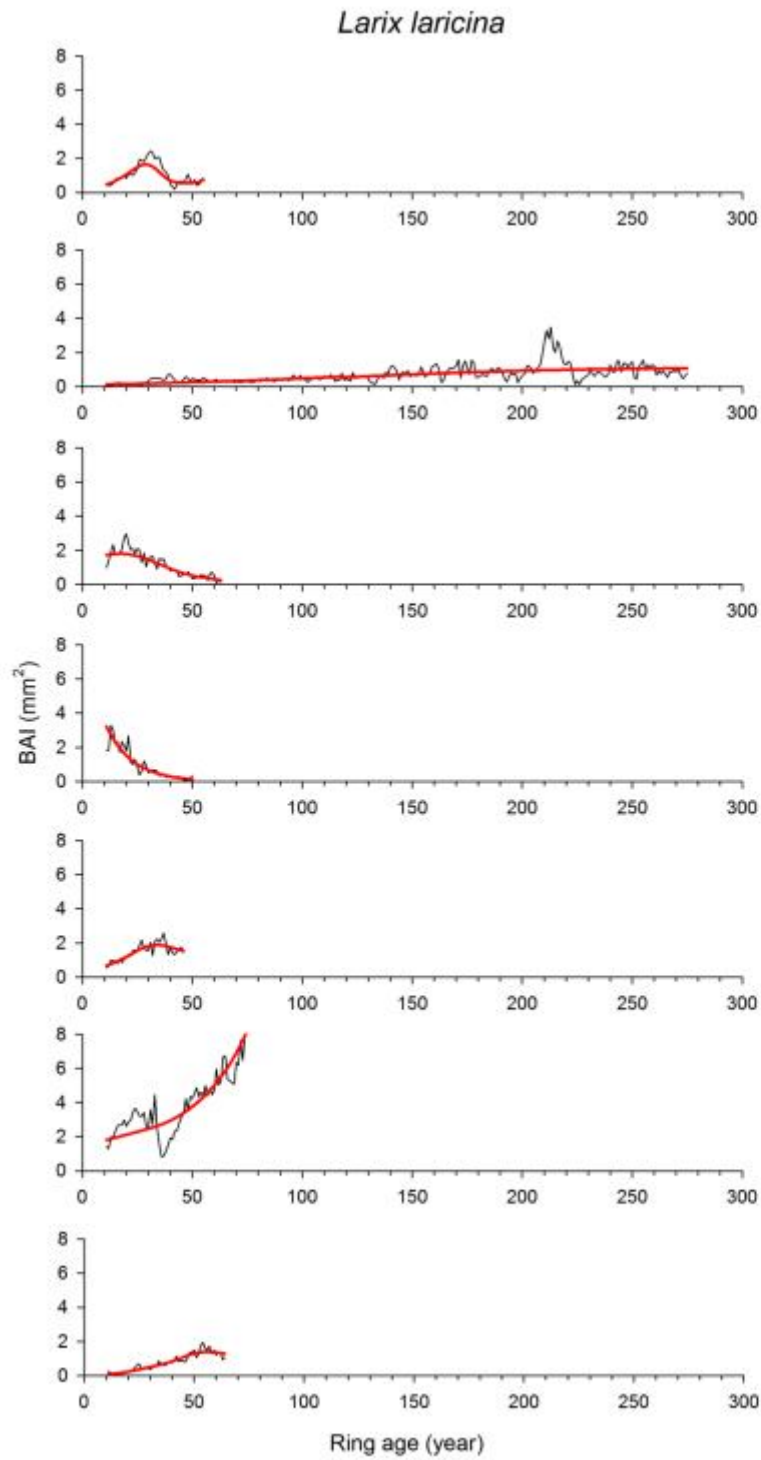


Figure S4. *Continues*

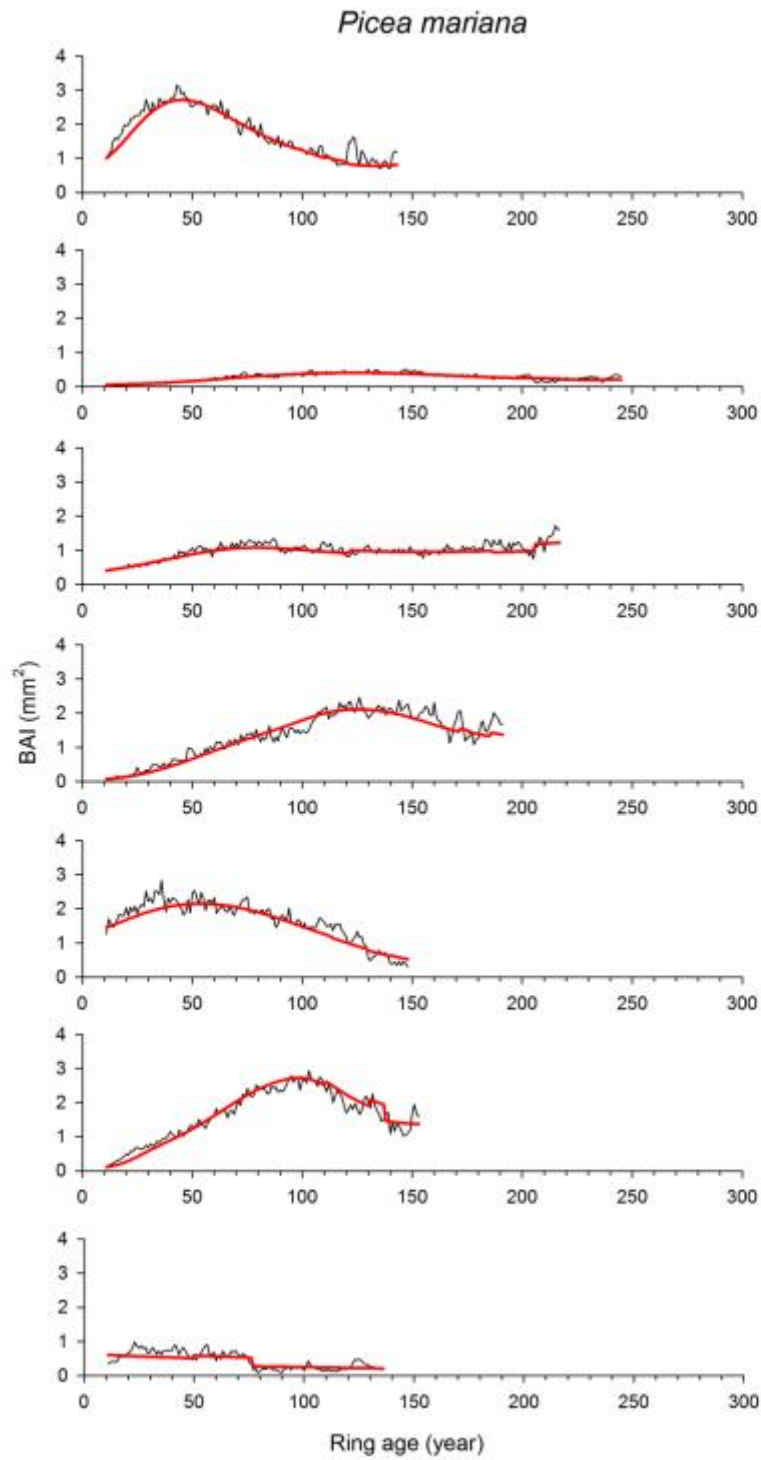


Figure S4. *Continues*

Growth in Canada's boreal forest

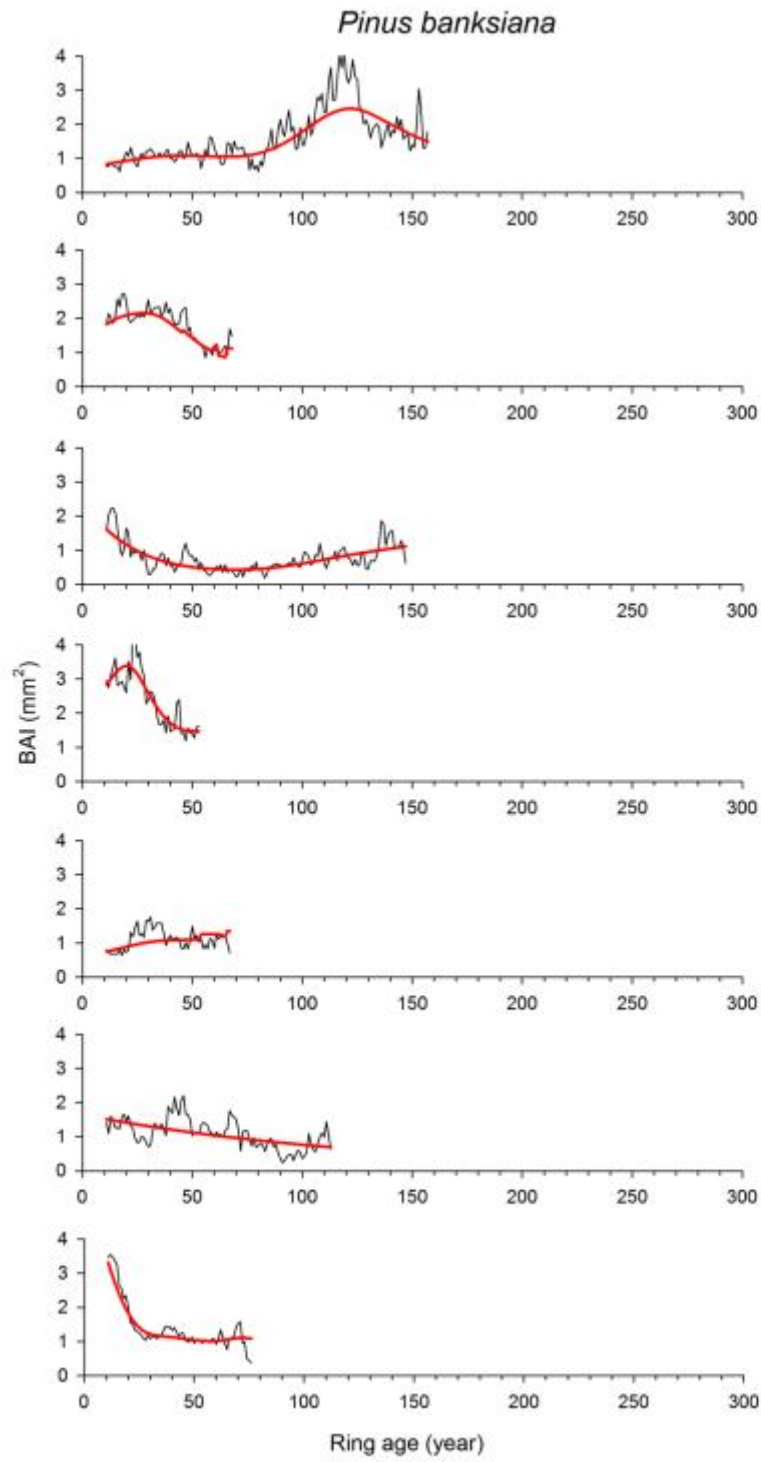


Figure S4. *Continues*

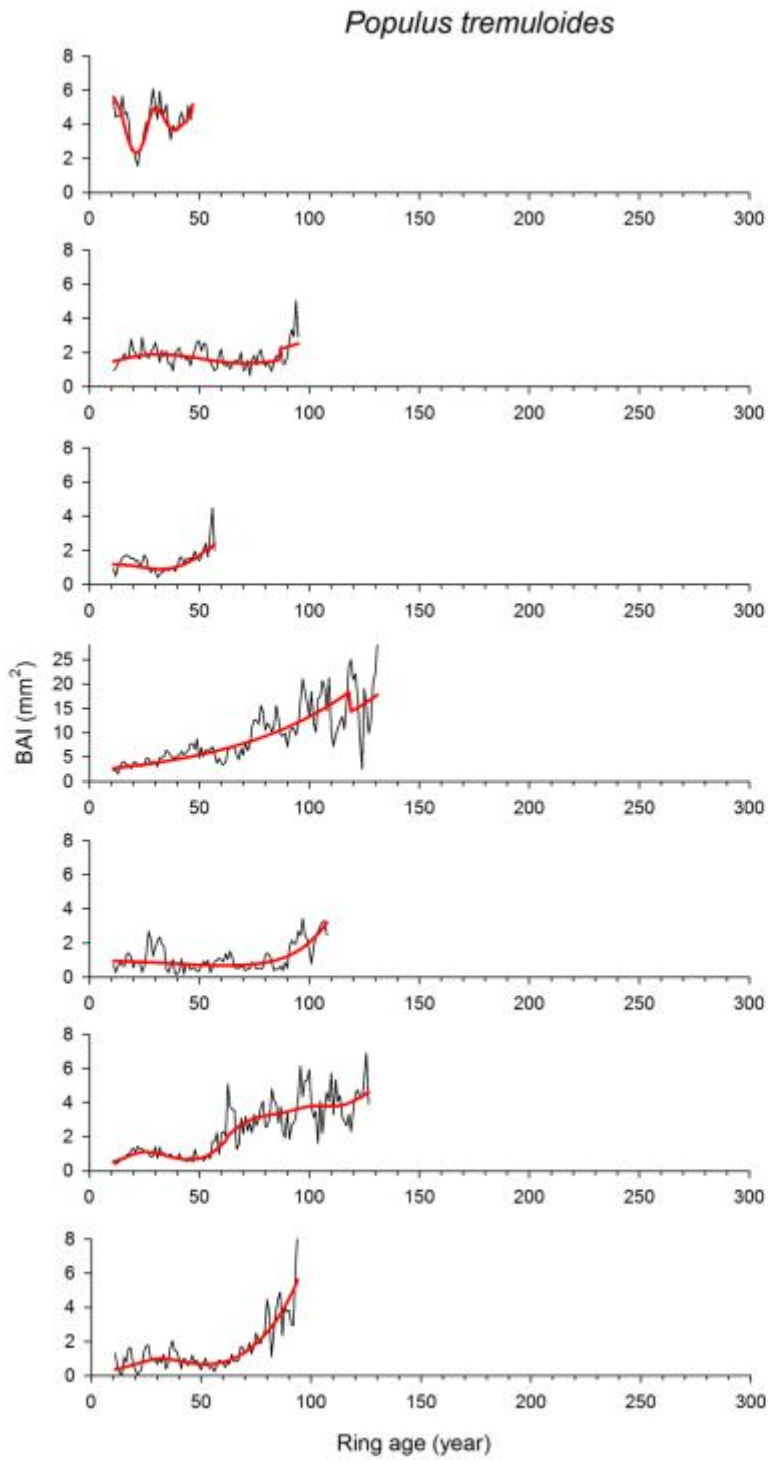


Figure S4. *Continues*

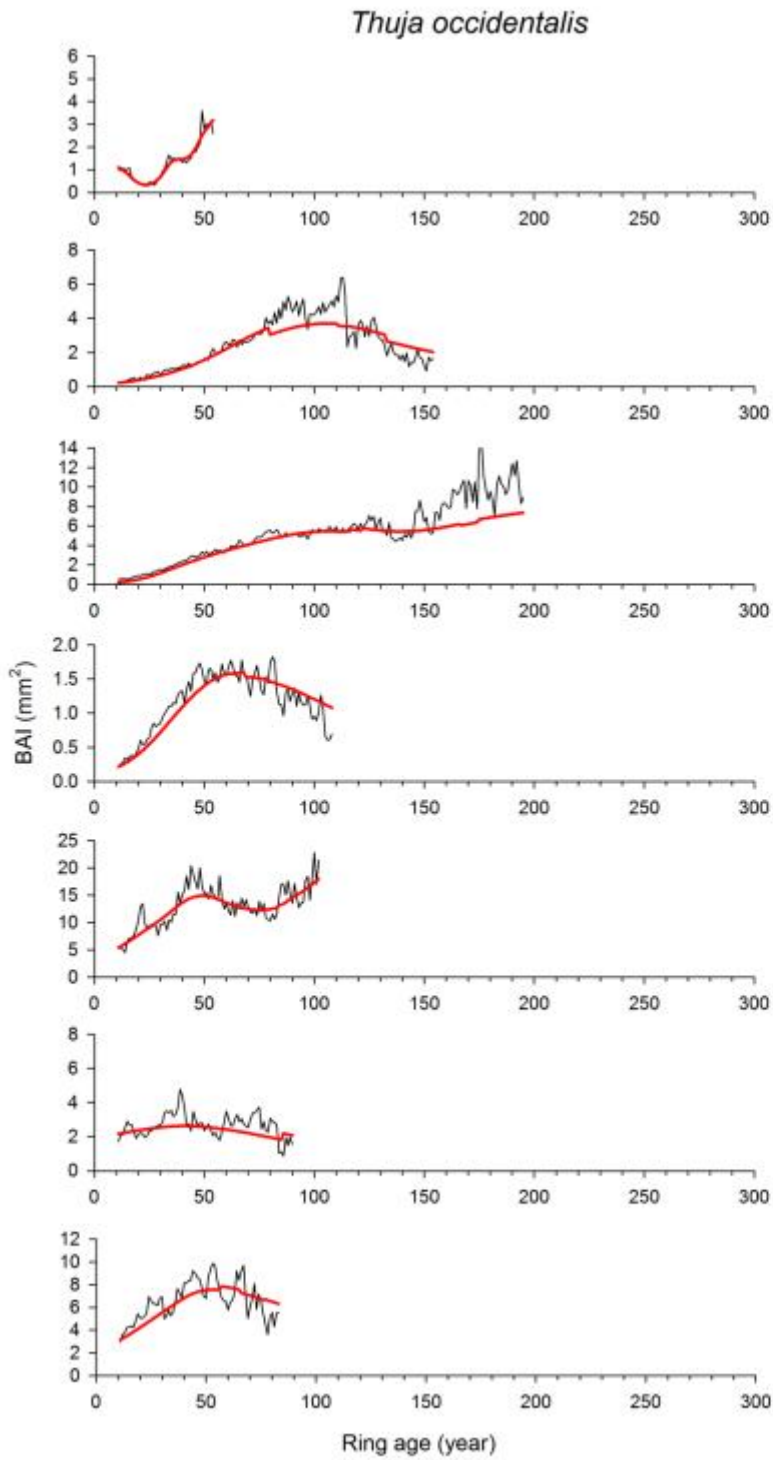


Figure S4. *Continues*

B.2 Generalized negative exponential (GNE) procedure

To assess the extent to which the choice of approach for removing age, size and competition effects might influence our conclusions, we also applied a tree level-based generalized negative exponential (GNE) statistical detrending procedure.

Here, the ring-width measurement series were rescaled using a power transformation method and detrended using three growth trend models, i.e., linear (L), negative exponential (NE), and generalized negative exponential (GNE) (12). The model to be retained for detrending was selected by a two-step comparison of the R^2 of the candidate models: the model with the highest R^2 between L and NE was selected; GNE was selected only if its R^2 was at least 5% higher than the R^2 of the model selected in the first step. The residuals of the observed minus fitted are hereafter referred to as the GNE growth reconstructions. Below are biplots of the fitted versus observed tree basal area increments generated using the plot-level GNE approach (Fig. S5).

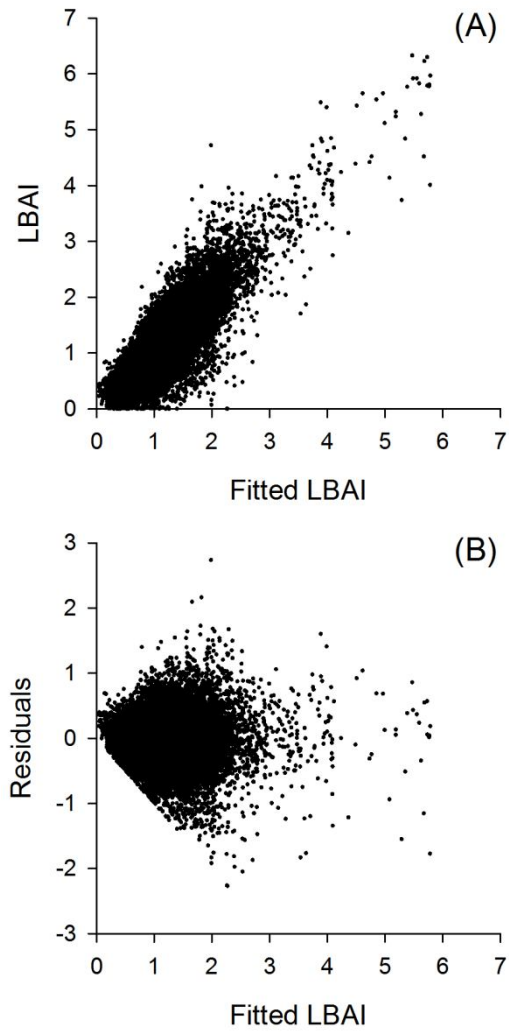


Figure S5. (A) Fitted versus observed log-scaled tree basal area increments (LBAI). The fitted values were those obtained from the Generalized Negative Exponential (GNE) models. (B) Residual versus fitted LBAI.

B.3 Generalized Additive Mixed Models and Regional Curve Standardization applied at the scale of ecozones

To assess the extent to which the choice of approach for removing age and size effects might influence our conclusions, we also applied two uniform ecozone-level procedures to generate two additional forms of tree growth indices: GAMMeco (model diagnostics in Table S2) and Regional Curve Standardization (RCS) (13). The regional curve standardization (RCS) technique has the potential to preserve the evidence of long-time scale forcing of tree growth as it scales ring-width measurements against an expectation of growth for the appropriate age of each ring (13)). This technique has already been successfully applied with success to *Pinus banksiana* in central (14) and eastern (15) boreal Canada.

As shown in Fig. 3 of the main text, and further highlighted by Table S2, there is evidence for key differences in results between the different approaches, notably for species such as *Abies balsamea*, *Picea glauca* and *Picea mariana*. Such differences can originate from computational variation of the tree-growth index. Notably, the RCS records were computed from the robust-weighted average of the detrended LBAI, whereas the GAMM records were computed from the average of the plot-level means of the detrended BAI (after rescaling into arithmetic unit). However, the GNE records were computed from the average of the plot-level means of LBAI. Therefore, some differences may be noted because of different approaches for aggregating the time series. Furthermore, tree distribution sometimes encompasses a variety of environmental conditions in terms of soil texture and moisture, organic layer depth, slope, stand density, etc. This may reduce the predictive power of the ecozone-level models and induce a bias in the aggregated detrended measurements. Diagnostics of the GAMM_{eco} (Table S2) suggest some bias in fitted vs observed slopes for *Abies balsamea*, *Picea glauca*, *Picea mariana* and *Larix laricina* (slope > 1.2). Nevertheless, the ecozone-level GAMM_{eco} records are similar to the plot-level GAMM_{NFI} records, and this is particularly true for the period post-1950 (Fig. 3 of the main text and Table S3).

Table S2. Diagnostics of the ecozone-level Generalized Additive Mixed Models (GAMM). The *r*-squared is computed from the square of the Pearson correlation between observed and predicted LBAI. The slope is computed from the linear regression of observed (y) LBAI as a function of predicted (x) LBAI. The amount of sampled rings for each GAMM is given by No. rings.

Species	Ecozone	<i>r</i> -squared	Slope	No. rings
<i>Abies balsamea</i>	Atlantic Maritime	0.091	1.234	1297
<i>Abies balsamea</i>	Boreal Shield East	0.436	1.604	7421
<i>Abies lasiocarpa</i>	Boreal Cordillera	0.817	1.059	3957
<i>Abies lasiocarpa</i>	Montane Cordillera	0.770	1.044	7420
<i>Acer saccharum</i>	Atlantic Maritime	0.591	1.077	1201
<i>Betula papyrifera</i>	Boreal Shield East	0.450	1.187	2760
<i>Larix laricina</i>	Boreal Plains	0.347	1.233	2385
<i>Larix laricina</i>	Boreal Shield East	0.696	1.219	1347
<i>Larix laricina</i>	Boreal Shield West	0.559	1.526	1125
<i>Larix laricina</i>	Taiga Plains	0.591	1.197	1288
<i>Picea engelmannii</i>	Montane Cordillera	0.734	1.078	1753
<i>Picea glauca</i>	Boreal Plains	0.592	1.258	3460
<i>Picea glauca</i>	Boreal Shield East	0.529	1.290	4034
<i>Picea glauca</i>	Taiga Plains	0.783	1.058	15693
<i>Picea mariana</i>	Atlantic Maritime	0.590	1.404	1683
<i>Picea mariana</i>	Boreal Plains	0.618	1.259	11660
<i>Picea mariana</i>	Boreal Shield East	0.579	1.263	47708
<i>Picea mariana</i>	Boreal Shield West	0.708	1.111	19684
<i>Picea mariana</i>	Taiga Plains	0.645	1.211	17397
<i>Pinus banksiana</i>	Boreal Plains	0.634	1.087	3199
<i>Pinus banksiana</i>	Boreal Shield East	0.756	1.061	3190
<i>Pinus banksiana</i>	Boreal Shield West	0.686	1.080	5085
<i>Pinus contorta</i>	Montane Cordillera	0.599	1.205	12661
<i>Pinus strobus</i>	Boreal Shield East	0.778	1.097	1475
<i>Populus tremuloides</i>	Boreal Plains	0.556	1.091	4631
<i>Populus tremuloides</i>	Boreal Shield East	0.567	1.172	1849
<i>Populus tremuloides</i>	Boreal Shield West	0.728	1.041	2149
<i>Populus tremuloides</i>	Taiga Plains	0.658	1.055	1130
<i>Thuja occidentalis</i>	Boreal Shield East	0.677	1.139	6925
<i>Thuja occidentalis</i>	Mixedwood Plains	0.738	1.117	1928
<i>Tsuga heterophylla</i>	Pacific Maritime	0.669	1.096	2314

PART C: Linear trends in forest growth from 1950 to 2002

Linear trends for 1950 to 2002 at the species-by-ecozone level were examined and direction was interpreted for the level of certainty: 'Very likely' if the sign of the trend in $GAMM_{NFI}$ was matched by the three other methods, 'Likely' if the sign of the trend in $GAMM_{NFI}$ was matched by two other methods, and 'Uncertain' if inconsistency was found between the methods; the term 'Inconclusive' was used when a trend in $GAMM_{NFI}$ was between 0 and $\pm 0.10\% \text{ yr}^{-1}$. Table S3 summarizes these species-by-ecozone analyses. Time-series of species-by-ecozone forest growth variability that were not presented in Fig. 3 but discussed in the main text are presented in Fig. S6.

Growth in Canada's boreal forest

Table S3. Linear trends in forest growth from 1950 to 2002. Analyses were performed on data originating from four methods of elimination of growth trends: species-by-plot and species-by-ecozone Generalized Additive Mixed Models (GAMM_{NFI} and GAMM_{eco}), generalized negative exponential (GNE) procedure, and Regional Curve Standardization (RCS). The slope (β) was determined from ordinary least-square regression on GAMM_{NFI}. β ranges from decreasing growth (negative) to increasing growth (positive). r is the Spearman rank correlation coefficient; values significant at the 5% level are in bold. The trend direction for $-0.10 > \beta > 0.10$ was interpreted for the level of uncertainty: ‘Very likely’ if the sign of the trend in GAMM_{NFI} is matched by the three other methods, ‘Likely’ if the sign of the trend in GAMM_{NFI} is matched by two other methods, and ‘Uncertain’ if inconsistency was found between the methods.

Ecozone Units	Species	β GAMM _{NFI} (% yr ⁻¹)	r GAMM _{NFI}	r GNE	r GAMM _{eco}	r RCS	N trees	Interpretation
Atlantic Maritime	<i>Abies balsamea</i>	-0.08	-0.123	-0.112	0.779	0.708	27	None
Atlantic Maritime	<i>Acer saccharum</i>	-0.02	-0.046	0.253	0.262	-0.398	20	None
Atlantic Maritime	<i>Picea mariana</i>	-0.10	-0.164	-0.043	-0.317	-0.209	32	Very likely
Boreal Cordillera	<i>Abies lasiocarpa</i>	+0.11	0.117	0.003	-0.202	0.413	34	Likely
Boreal Plains	<i>Larix laricina</i>	+0.49	0.329	0.379	0.830	0.754	24	Very likely
Boreal Plains	<i>Picea glauca</i>	+0.30	0.453	0.059	0.626	0.495	76	Very likely
Boreal Plains	<i>Picea mariana</i>	-0.11	-0.220	-0.202	0.120	0.174	170	Uncertain
Boreal Plains	<i>Pinus banksiana</i>	+0.29	0.345	0.333	0.599	0.248	54	Very likely
Boreal Plains	<i>Populus tremuloides</i>	-0.15	-0.165	-0.030	0.053	0.054	98	Uncertain
Boreal Shield East	<i>Abies balsamea</i>	+0.00	0.064	0.092	0.55	0.524	138	None
Boreal Shield East	<i>Betula papyrifera</i>	+0.12	0.089	-0.159	-0.259	-0.01	37	Uncertain
Boreal Shield East	<i>Larix laricina</i>	-0.03	0.251	0.198	0.377	0.698	32	None
Boreal Shield East	<i>Picea glauca</i>	+0.12	0.169	0.003	0.59	0.558	55	Very likely
Boreal Shield East	<i>Picea mariana</i>	-0.16	-0.373	-0.528	-0.668	-0.667	530	Very likely
Boreal Shield East	<i>Pinus banksiana</i>	-0.17	-0.204	-0.16	0.193	-0.196	56	Likely
Boreal Shield East	<i>Pinus strobus</i>	-0.17	-0.148	-0.154	0.154	-0.059	21	Likely
Boreal Shield East	<i>Populus tremuloides</i>	+0.15	0.080	-0.102	-0.275	-0.241	34	Uncertain
Boreal Shield East	<i>Thuja occidentalis</i>	-0.49	-0.549	-0.543	-0.719	-0.784	76	Very likely
Boreal Shield West	<i>Larix laricina</i>	+0.13	0.159	0.169	0.782	0.809	20	Very likely
Boreal Shield West	<i>Picea mariana</i>	+0.11	0.118	-0.118	-0.394	-0.209	268	Uncertain
Boreal Shield West	<i>Pinus banksiana</i>	+0.01	-0.023	-0.203	-0.37	-0.135	84	None
Boreal Shield West	<i>Populus tremuloides</i>	+0.04	0.013	0.103	-0.163	-0.321	30	None
Mixedwood Plains	<i>Thuja occidentalis</i>	-0.16	-0.161	0.051	-0.394	-0.395	35	Likely
Montane Cordillera	<i>Abies lasiocarpa</i>	+0.17	0.231	0.274	-0.164	0.247	61	Likely
Montane Cordillera	<i>Picea engelmannii</i>	-0.14	-0.116	-0.420	-0.224	0.321	21	Likely
Montane Cordillera	<i>Pinus contorta</i>	+0.38	0.538	0.127	0.293	0.31	147	Very likely
Pacific Maritime	<i>Tsuga heterophylla</i>	-0.66	-0.613	0.001	-0.719	0.429	24	Uncertain

Growth in Canada's boreal forest

Taiga Plains	<i>Larix laricina</i>	-0.26	-0.186	-0.385	-0.823	-0.57	21	Very likely
Taiga Plains	<i>Picea glauca</i>	-0.12	-0.245	-0.050	-0.184	0.129	131	Likely
Taiga Plains	<i>Picea mariana</i>	-0.10	-0.225	-0.165	-0.653	-0.750	196	Very likely
Taiga Plains	<i>Populus tremuloides</i>	-0.21	-0.118	0.023	-0.010	0.372	21	Uncertain

Significance was tested against the null hypothesis that the trend is different from zero, using a variant of the t test with an estimate of the effective sample size that takes into account the presence of serial persistence in data (16), (their sections 8.2.3 and 6.6.8).

Growth in Canada's boreal forest

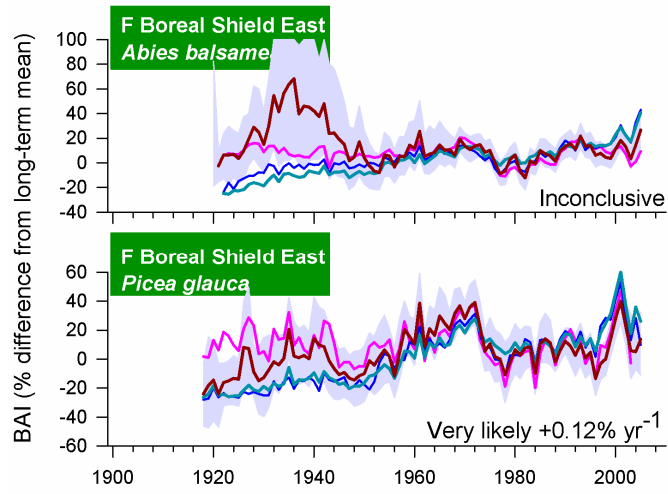


Figure S6. Species-by-ecozone forest growth variability assessed from tree-ring measurement series for *Picea glauca* and *Abies balsamea* in the eastern Boreal Shield.

PART D: Relationship between normalized difference vegetation index and forest growth

As seen in the main text, the spatial patterns of growth trends identified in our analysis of tree-rings were to some extent coherent with the trends estimated by remote sensing (e.g., eastern and northwest forests), but there are areas where in situ data did not match the remote sensing information (e.g., western forests). For each $1^\circ \times 1^\circ$ grid point, annual time series of forest growth changes (GAMM_{NFI}) were correlated with annually averaged normalized difference vegetation index (NDVI) data down-sampled to a $1^\circ \times 1^\circ$ resolution. The period for the pointwise correlation was 1982 to 2002. To be consistent with the year-to-year carbohydrate mobilization (17) (18) (19) (20), the pointwise correlation analysis was repeated on backward and forward lags of GAMM_{NFI} . The maximum correlation values computed among the three iterations (backward, current and forward lags) at each grid were then used to create a spatial correlation map for the goodness-of-fit. The null hypothesis of no significant relationship between GAMM_{NFI} and NDVI was rejected at the 10% level (one-sided test) when $r > 0.291$. The pointwise correlation analysis was repeated after applying a first difference transformation to remove trends, positive autocorrelation and temporal drifts in NDVI and tree-ring data. The results for four selected pixels across a longitudinal gradient are presented in Fig. S7. The selection of pixels was made based on the noted improvement of the fit after first differencing. This suggests coherence between growth and NDVI at high frequencies but not at lower frequencies.

Growth in Canada's boreal forest

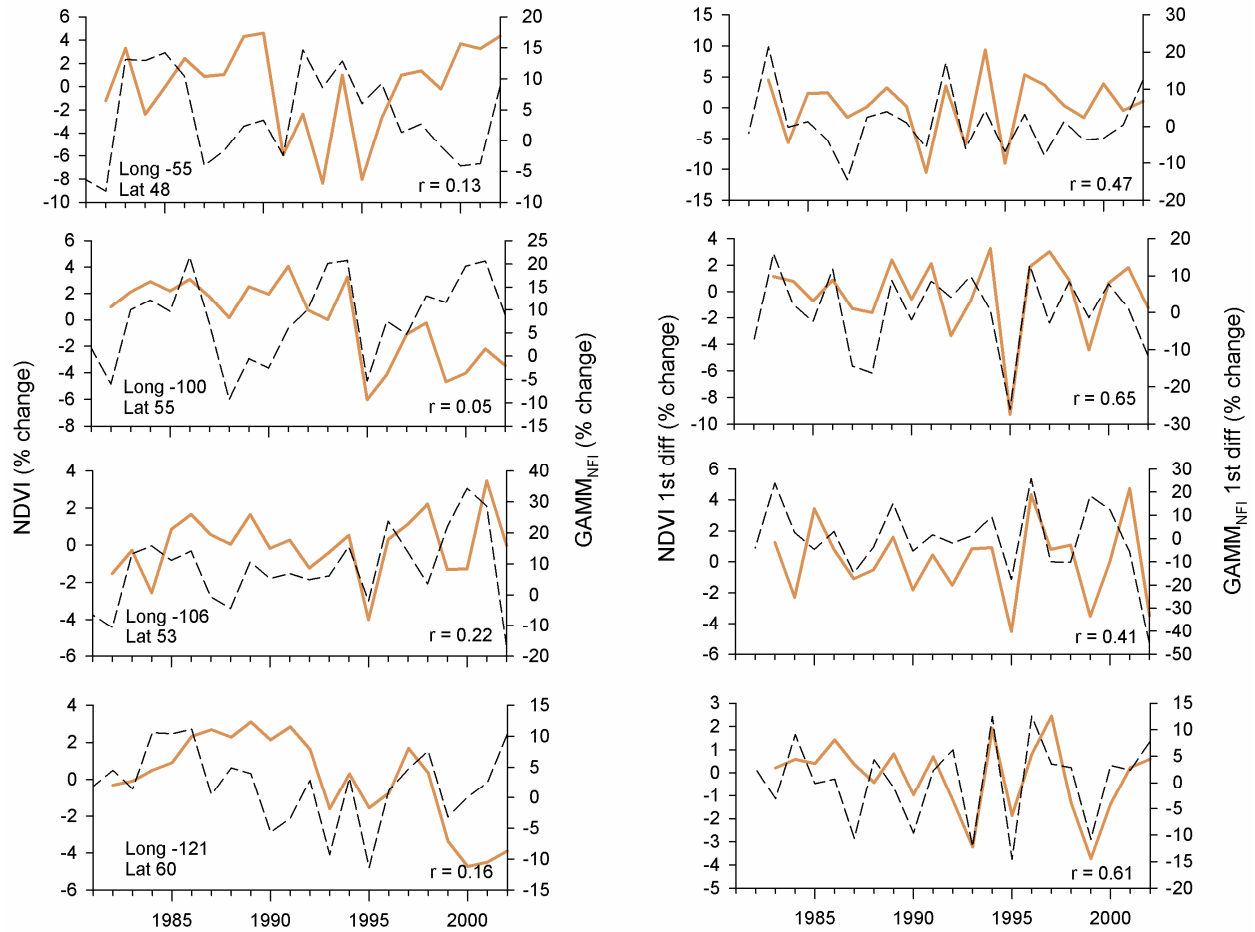


Figure S7. Growth versus NDVI time-series. *Left column:* Examples of NDVI and $GAMM_{NFI}$ time-series for four selected pixels across a longitudinal gradient. *Right column:* Same after the application of a first difference transformation to the data. Estimates are expressed as percent change relative to the long-term average.

PART E: Relationship between atmospheric drought and forest growth

Below we report on trends in spring (February-April), summer (June-August) and fall (September-November) temperatures, cool season snowfall (November-April), summer relative humidity, and summer vapor pressure deficit for each $1^\circ \times 1^\circ$ grid (Figs. S8 and S9). Note that one should be cautious when interpreting the maps because relatively few stations report on relative humidity. Hence, there is a high level of extrapolation (and thus reduced spatial variability). In contrast, precipitation amounts are spatially variable (high variation across small spatial scales) and are routinely measured across Canada's climate station network, thereby inducing more reliable estimation of spatial variation in the soil moisture index (SMI) product (Fig. 5 of the main text).

Growth in Canada's boreal forest

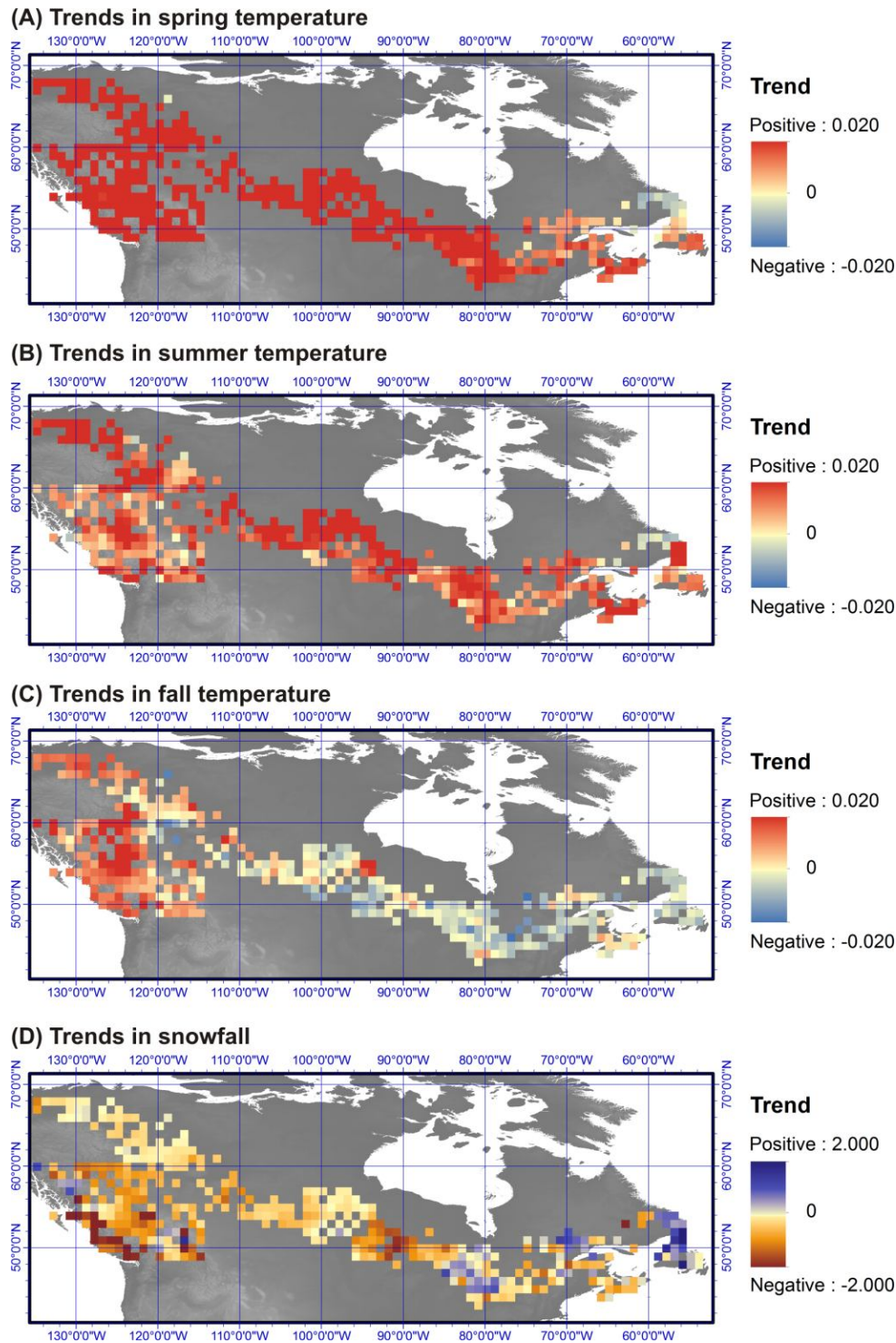


Figure S8. Spatial distribution of trends in A) spring (March-May, trends expressed in $^{\circ}\text{C yr}^{-1}$), B) summer (June-August) and C) fall (September-November) mean temperature, and D) total winter snowfall (December-May, mm of water yr^{-1}) across sampled NFI locations from 1950 to 2002. Maps show strong spring warming west of 80°W , summer warming across much of the area, fall warming over the Montane Cordillera, and heterogeneous snowfall patterns.

Growth in Canada's boreal forest

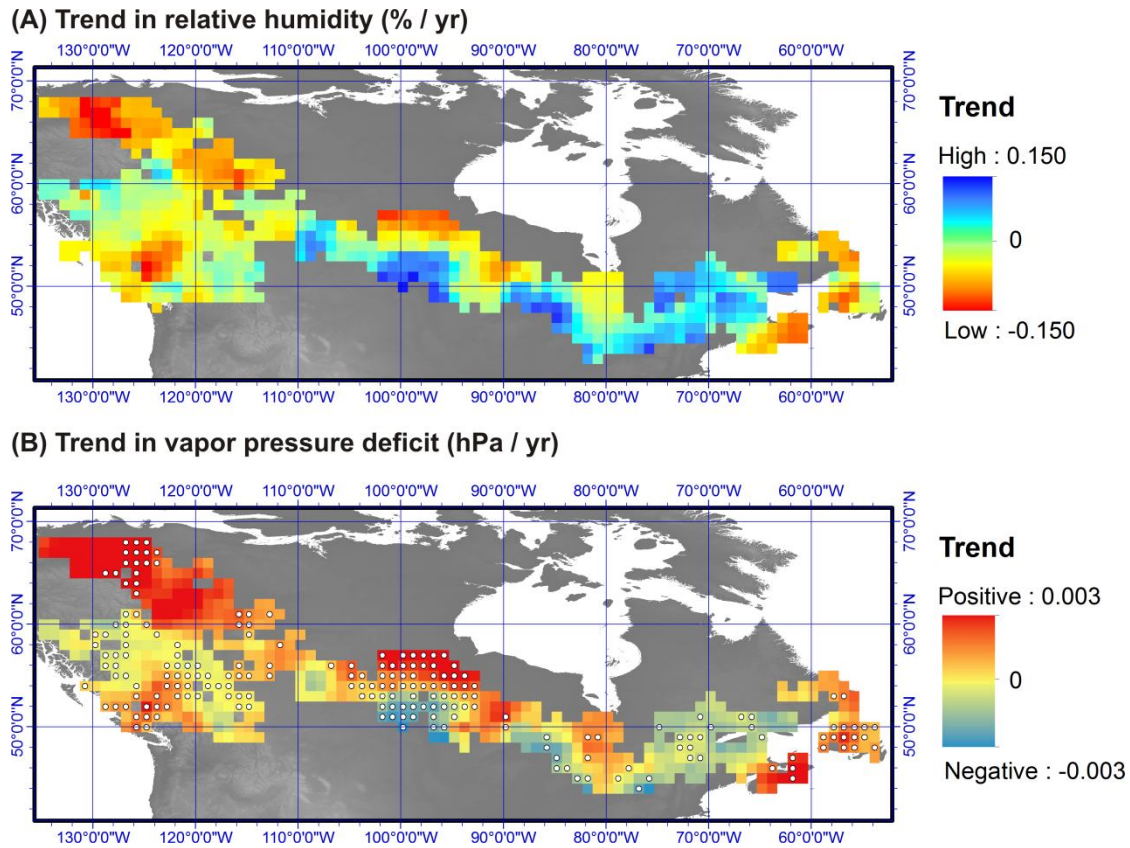


Figure S9. Spatial distribution of trends in A) relative humidity ($\% \text{ yr}^{-1}$) and B) vapor pressure deficit (VPD, kPa yr^{-1}) for the summer months of June to August across Canada from 1950 to 2002. Dots on map (B) indicate areas for which trends in VPD and GAMM_{NFI} (Fig. 2B of the main text) were of opposite signs (i.e., the expected response where increasing VPD is accompanied by decreasing growth, or where decreasing VPD is accompanied by increasing growth).

PART F: Linear mixed models for climate sensitivity

Linear mixed models were used to explore climate effects on species-by-plot averaged residuals of eq. 2 ($GAMM_{LResijt}$). Collinearity amongst the input variables may be a source of problem in mixed models. Here, we examined for collinearity by calculating Pearson correlation coefficients between explanatory variables at each NFI locations, and averaging results for the whole study area. As shown in Table S4, collinearity amongst the variables is generally low (absolute value of $r < 0.4$); hence, no variable was excluded following this examination.

Also shown below are the proportions of the subset-averaged coefficients that exceeded the 95% adjusted confidence interval in the linear mixed effect models (Table S5), and a map of grid-by-grid correlation between observed and fitted $GAMM_{LResijt}$ data (Fig. S10).

Furthermore, analyses performed on the species-by-ecozone $GAMM_{eco}$ chronologies were made to double-check the plot-level analysis with regard to the CO_2 results. Therein, species-by-ecozone linear mixed models were used to explore the climate and CO_2 effects on tree-sample residuals of the species-by-ecozone $GAMM$ models ($GAMM_{eco}$). In total, for these analyses, there were 47 combinations of species and ecozones. The model structure was essentially the same as the one described in the main text, except the models were run at the tree level with trees as random factor. The results support the conclusions derived from the species-by-plot analyses, with CO_2 being positively significant in a small subset of the analyses (7 positively tested versus 47 tests in total; Fig. S11).

Growth in Canada's boreal forest

Table S4. Means of the Pearson correlations between explanatory variables.

	<i>SummerT</i> _(t)	<i>SpringT</i> _(t)	<i>SummerT</i> _(t-1)	<i>FallT</i> _(t-1)	<i>SoilWater</i> _(t)	<i>SoilWater</i> _(t-1)	<i>Snowfall</i>	CO ₂
<i>SummerT</i> _(t)	1.00							
<i>SpringT</i> _(t)	0.21	1.00						
<i>SummerT</i> _(t-1)	0.11	0.07	1.00					
<i>FallT</i> _(t-1)	0.11	0.06	0.12	1.00				
<i>SoilWater</i> _(t)	-0.36	-0.07	-0.06	-0.03	1.00			
<i>SoilWater</i> _(t-1)	0.05	0.03	-0.37	0.02	0.19	1.00		
<i>Snowfall</i>	-0.11	-0.38	0.01	-0.07	0.11	0.00	1.00	
[CO ₂]	0.30	0.32	0.28	0.16	0.02	0.03	-0.21	1.00

Abbreviations of climatic variables: *SummerT*, summer temperature; *SoilWater*, summer soil water; *FallT*, fall temperature; *SpringT*, spring temperature; *Snowfall*, cool season total snowfall; CO₂, atmospheric CO₂ concentrations. Terms *t-1* and *t* describe influences taking place the previous year and current year to ring formation, respectively.

Growth in Canada's boreal forest

Table S5. Proportion (%) of the subset-averaged coefficients that exceed the 95% adjusted confidence intervals. See Table S4 for variable names. Negative and positive refer to the sign of the relationship.

Species	Summer $T_{(t)}$		Spring $T_{(t)}$		Summer $T_{(t-1)}$		Fall $T_{(t-1)}$		SoilWater $_{(t)}$		SoilWater $_{(t-1)}$		Snowfall		[CO ₂]	
	Negative	Positive	Negative	Positive	Negative	Positive	Negative	Positive	Negative	Positive	Negative	Positive	Negative	Positive	Negative	Positive
<i>Abies balsamea</i>	0	6	8	3	6	0	5	6	0	12	2	18	3	0	5	3
<i>Abies lasiocarpa</i>	0	13	6	3	23	0	0	35	10	0	0	26	6	6	10	13
<i>Acer rubrum</i>	0	21	14	0	7	0	0	7	7	29	7	14	7	0	7	0
<i>Acer saccharum</i>	0	20	0	0	20	0	0	0	0	0	0	0	0	0	20	0
<i>Betula alleghaniensis</i>	0	29	0	0	0	0	0	14	0	14	0	0	0	0	0	0
<i>Betula papyrifera</i>	0	27	0	0	18	0	9	0	0	0	0	0	0	27	0	0
<i>Larix laricina</i>	12	2	0	0	5	2	0	2	5	10	10	0	7	0	0	0
<i>Picea engelmannii</i>	0	13	0	13	13	0	0	0	0	38	0	38	0	13	0	0
<i>Picea glauca</i>	1	12	9	2	15	2	3	4	2	13	4	7	6	1	4	5
<i>Picea mariana</i>	3	9	3	12	20	0	3	6	0	19	4	7	4	2	10	6
<i>Pinus banksiana</i>	0	11	0	12	20	0	0	8	2	23	0	6	12	0	5	0
<i>Pinus contorta</i>	2	7	0	14	5	0	0	19	0	33	0	9	12	5	9	7
<i>Pinus strobus</i>	0	0	0	25	0	0	13	13	0	75	0	0	25	0	0	0
<i>Populus balsamifera</i>	0	0	0	0	38	0	13	0	0	25	13	0	13	0	0	0
<i>Populus tremuloides</i>	2	14	3	8	9	0	20	0	0	18	2	17	3	6	0	2
<i>Pseudotsuga menziesii</i>	0	0	0	25	25	0	0	0	0	100	0	0	25	0	0	0
<i>Thuja occidentalis</i>	12	4	0	32	20	0	0	0	0	20	0	20	4	0	12	4
<i>Thuja plicata</i>	0	0	0	0	0	9	0	18	0	18	0	18	9	0	0	9
<i>Tsuga heterophylla</i>	0	0	0	20	0	0	0	10	20	0	0	10	0	0	20	0
Total	3	10	4	9	15	1	4	7	1	18	3	10	6	2	7	4

Growth in Canada's boreal forest

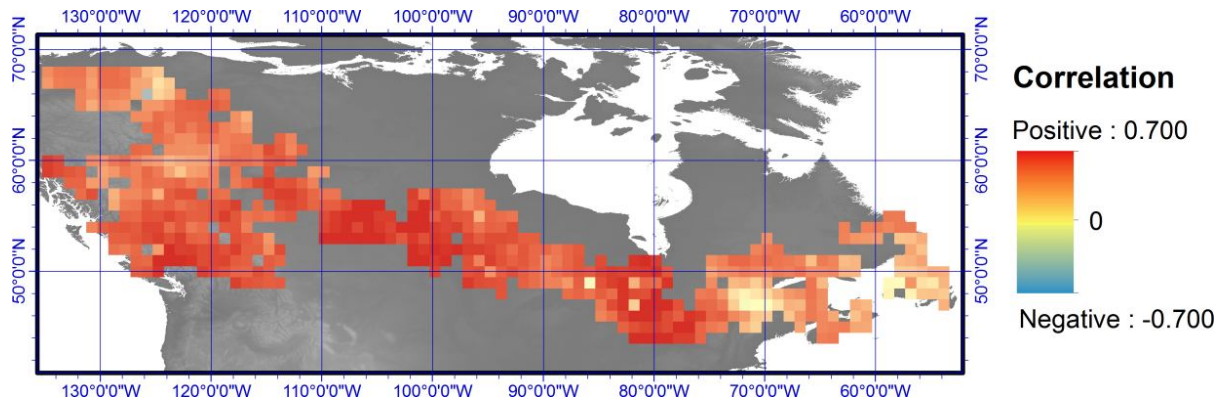


Figure S10. Spatial distribution of correlations between interpolated forest growth (GAMM_{NFI}) and changes predicted by the linear mixed models. GAMM_{NFI} and predictions were interpolated to 1° x 1° grids to obtain continuous yearly raster maps of predicted growth covering 1950 to 2002. For each 1°×1° grid point, annual time series of GAMM_{NFI} were correlated with predictions. The period for the pointwise correlation was 1950 to 2002. The median of mapped correlation coefficients is $r = 0.497$, with 25th and 75th percentiles equaling $r = 0.393$ and $r = 0.592$, respectively.

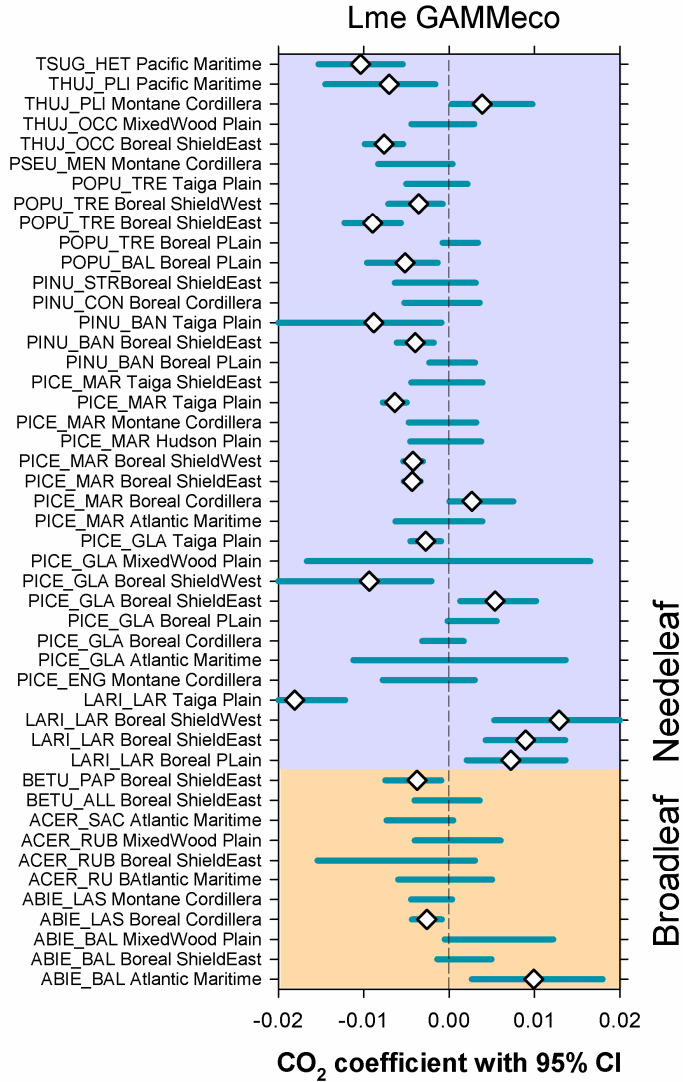


Figure S11. Species-by-ecozone linear mixed model 95% adjusted confidence intervals for the influence of atmospheric CO₂ concentrations on basal area increment. Values exceeding the probability level are identified by a diamond.

PART G: Additional material

In our main results, species-by-plot GAMM_{NFI} chronologies were computed using robust averages of the detrended individual tree BAI data. These were then spatially-averaged to $1^\circ \times 1^\circ$ grids using Kriging to obtain continuous yearly raster maps of growth covering 1950 to 2002 (i.e., the period of maximum sample replication). However, we were initially concerned that stands having few sampled trees, and stands made up of young trees or rare tree species, might tend to lower the low-frequency variance in the overall regional chronology, thus posing difficulties for the detection of growth trends. Below we present an analysis in which rare species and plots containing low sampled years were excluded. In this analysis, all species by plot chronologies were reprocessed through plot-level Generalized Additive Mixed Models (GAMM_{NFI}) after excluding chronologies made up of fewer than four trees and/or spanning less than 53 years. Kriging was then rerun and trends were recomputed to recreate maps similar to those in Fig. 2. In total, 256 species by plot chronologies were retained in this analysis. As expected, the reduced sample sizes led to an increase in spatial smoothing, thus contributing to reduced correlation with the original maps. Furthermore, the removal of samples from the most poorly represented areas would tend to reduce the reliability of interpolations in those areas. Yet, the conclusion with regard to regional and global trends was not very different from the original one (Fig. S12): the trend computed on the country-wide averaged growth data was not significant, albeit fairly close to being negative (see caption of Fig. S12). Note that in these analyses, the retained samples were more heavily weighted toward long-lived black spruce, which made up 52% of the chronologies.

The design of the GAMM_{NFI} detrending method (and even more so of the GNE) will tend to remove long-term growth trends of a period longer than the optimal spline flexibility for poorly sampled stands. Any stand where a certain cambial age is represented by only one or a few trees will naturally have its temporal trends removed (because tree age/size and time are often correlated). One way to partly address this issue is to increase the spatial scale of the analyses. Below we present spatial distributions of forest growth trends across Canada derived from species-by-plot chronologies obtained from the Generalized Additive Mixed Models applied at the ecozone scale (GAMM_{eco}). This approach was not prioritized in our original work because these GAMM_{eco} models showed evidence of bias (Table S2). The conclusion from this analysis with regard to regional and global trends was not very different from the original one: regionally, the 1982 to 2002 map is very coherent with the one presented in the main paper (Fig. S13). This is less so for the 1950-2002 maps, yet they are still similar. The dissimilarity is particularly evident in the east, and this is essentially where the GAMM_{eco} models were showing greater bias (Boreal Shield east and Atlantic Maritime ecozones, Supplementary Material Table S2). The amplitude of trends is larger here than in the main figure (as expected), but the trend computed on the country-wide averaged growth data was not significant (the country-wide averaged growth trend over 1950-2002 is $0.054\% \text{ yr}^{-1}$, $r = 0.15$ with 95% CI [-0.67, 0.80]), which supports the main conclusion of the paper about compensating effects).

Growth in Canada's boreal forest

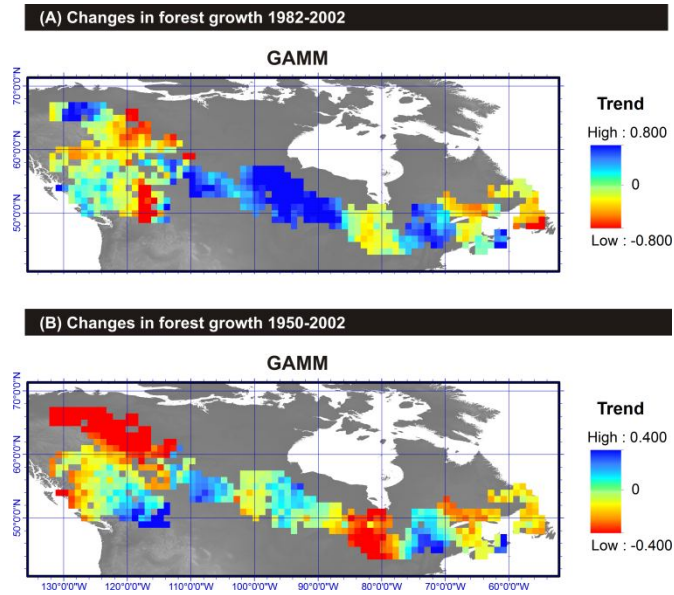


Figure S12. Spatial distribution of forest growth trends across Canada. Tree data were processed through pre-selected plot-level Generalized Additive Mixed Models ($GAMM_{NFI}$; trends are expressed in $\% \text{ yr}^{-1}$). Species by plot chronologies made up of less than four trees and spanning less than 53 years were excluded; 256 chronologies remained (black dots on maps). Trends estimated through the analyses of NFI tree cores for the periods of (A) 1982-2002 and (B) 1950-2002. The Spearman correlation between the map in (A) and the $GAMM_{NFI}$ map in Fig. 2A of the main text is $r = 0.38$. The Spearman correlation between the map in (B) and the $GAMM_{NFI}$ map in Fig. 2B of the main text is $r = 0.70$. The country-wide averaged growth trend in (B) is $-0.10\% \text{ yr}^{-1}$ ($r = -0.36$ with 95% CI $[-0.64, 0.01]$).

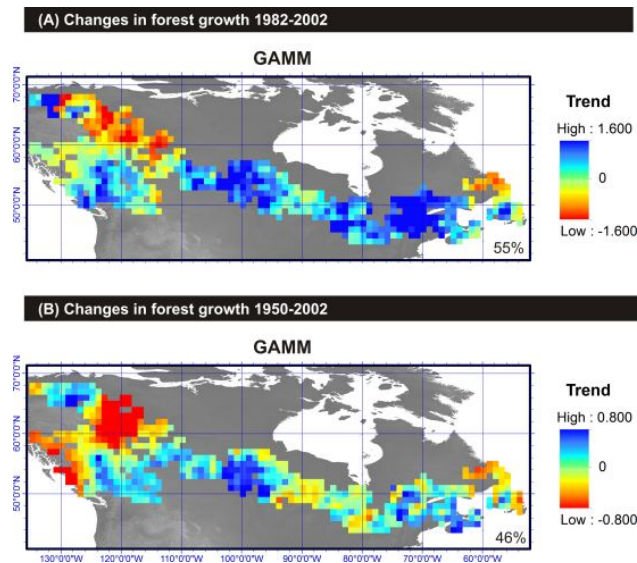


Figure S13. Spatial distribution of forest growth trends across Canada. Tree data were processed through ecozone-level Generalized Additive Mixed Models ($GAMM_{eco}$; trends are expressed in $\% \text{ yr}^{-1}$). Trends estimated through the analyses of NFI tree cores for the periods of (A) 1982-2002 and (B) 1950-2002. The Spearman correlation between the map in (A) and the $GAMM_{NFI}$

map in Fig. 2A of the main text is $r = 0.62$. The Spearman correlation between the map in (B) and the GAMM_{NFI} map in Fig. 2B of the main text is $r = 0.43$.

References

1. Gillis MD, Omule AY, Brierley T (2005) Monitoring Canada's forests: the National Forest Inventory. *For Chron* 81:214–221.
2. Larsson L (2013) *CooRecorder and Cdendro programs of the CooRecorder/Cdendro package (version 7.6)*. Cybis Elektronik & Data AB, Saltsjöbaden, Sweden. <http://www.cybis.se>.
3. Yamaguchi DK (1991) A simple method for cross-dating increment cores from living trees. *Can J For Res* 21:414–416.
4. Holmes RL (1983) Computer-assisted quality control in tree-ring dating and measurement. *Tree-Ring Bull* 43:69–78.
5. Olson DM, et al. (2001) Terrestrial ecoregions of the world: a new map of life on earth. *BioScience* 51:933–938.
6. National Climate Data Center (2014) *International Tree-Ring Data Bank*. World Data Center for Paleoclimatology. Boulder, CO, USA.
7. Girardin M-P, Tardif JC, Flannigan MD, Bergeron Y (2006) Synoptic-scale atmospheric circulation and boreal Canada summer drought variability of the past three centuries. *J Clim* 19:1922–1947.
8. Girardin MP (2010) Wildfire risk inferred from tree rings in the Central Laurentians of boreal Quebec, Canada. *Dendrochronologia* 28:187–206.
9. Wood SN (2006) *Generalized Additive Models: An Introduction With R*. Chapman Hall/CRC Press, Boca Raton, FL, USA.
10. Camarero JJ, Gazol A, Galván JD, Sangüesa-Barreda G, Gutiérrez E (2015) Disparate effects of global-change drivers on mountain conifer forests: warming-induced growth enhancement in young trees vs. CO₂ fertilization in old trees from wet sites. *Glob Change Biol* 21:738–749.
11. Baskerville GL (1972) Use of logarithmic regression in the estimation of plant biomass. *Can J For Res* 2:49–53.
12. Girardin MP, Guo XJ, de Jong R, Kinnard C, Bernier PY, Raulier F (2014) Unusual forest-growth decline in boreal North America covarying with the retreat of Arctic sea ice. *Global Chang Biol* 20:851–866.
13. Esper J, Cook E, Krusic P, Peters K, Schweingruber F (2003) Tests of the RCS method for preserving low-frequency variability in long tree-ring chronologies. *Tree-Ring Res* 59:81–98.

14. Girardin MP, Bernier PY, Raulier F, Tardif JC, Conciatori F, Guo XJ (2011) Testing for a CO₂ fertilization effect on growth of Canadian boreal forests. *J Geophys Res* 116:G01012.
15. Girardin MP, Guo JX, Bernier PY, Raulier F, Gauthier S (2012) Changes in growth of pristine boreal North American forests from 1950 to 2005 driven by landscape demographics and species traits. *Biogeosciences* 9:2523–2536.
16. von Storch H, Zwiers FW (1999) *Statistical Analysis in Climate Research*. Cambridge University Press, 484 pp.
17. Misson L (2004) MAIDEN: a model for analyzing ecosystem processes in dendroecology. *Can J For Res* 34:874–887.
18. Wettstein JJ, Littell JS, Wallace JM, Gedalof Z (2011) Coherent region-, species-, and frequency-dependent local climate signals in Northern Hemisphere tree-ring widths. *J Clim* 24, 5998–6012.
19. Babst F, Bouriaud O, Alexander R, Trouet V, Frank D (2014) Toward consistent measurements of carbon accumulation: A multi-site assessment of biomass and basal area increment across Europe. *Dendrochronologia* 32 :153–161.
20. Deslauriers A, Beaulieu M, Balducci L, Giovannelli A, Gagnon MJ, Rossi S (2014) Impact of warming and drought on carbon balance related to wood formation in black spruce. *Ann Bot* 114:335–345.